SPANWISE FLOW STRUCTURES WITHIN A LAMINAR SEPARATION BUBBLE ON AN AIRFOIL

Theodoros Michelis
Faculty of Aerospace Engineering
Delft University of Technology
t.michelis@tudelft.nl
Kluyverweg 2, 2629HT, Delft,
The Netherlands

Marios Kotsonis
Faculty of Aerospace Engineering
Delft University of Technology
m.kotsonis@tudelft.nl
Kluyverweg 2, 2629HT, Delft,
The Netherlands

Serhiy Yarusevych
Department of Mechanical and Mechatronics Engineering
University of Waterloo
syarus@uwaterloo.ca
200 University Ave. W, Waterloo, Ontario, Canada, N2L 3G1

ABSTRACT

The present study considers the development of a Laminar Separation Bubble on the suction side of a NACA0018 airfoil under natural and forced conditions. Deterministic forcing is applied by means of a two-dimensional plasma actuator installed on the airfoil surface. The spatio-temporal characteristics of the bubble are measured using time-resolved, two-component Particle Image Velocimetry in streamwise and spanwise planes. Analysis of the results shows that while the time-average bubble is strongly two-dimensional, the dominant coherent structures assume three dimensional organisation in the vicinity of laminar-turbulent breakdown in both natural and forced conditions.

INTRODUCTION

A Laminar Separation Bubble (LSB) develops if a laminar boundary layer is subjected to a sufficiently strong adverse pressure gradient. This causes separation, with subsequent laminar to turbulent transition of the shear layer. Increased mixing and energising of the separated shear layer results in time-averaged reattachment, thus creating the LSB (e.g. Jones *et al.*, 2010). This phenomenon is common on the suction side of airfoils at low Reynolds numbers based on chord length ($Re_c < 500,000$). It is relevant for a variety of industrial applications spanning from unmanned aerial vehicles to gliders and wind turbine blades. Since a LSB is inherently unstable, it can lead to unwanted dynamic effects such as stall, lift reduction, drag increase and noise production. Consequently, detailed description of the dynamics of LSBs is essential in order to effectively control them and has been a topic of extensive studies (e.g. Marxen & Henningson, 2011).

It is generally accepted that transition in the separated shear layer is governed by convective amplification of disturbances due to a Kelvin-Helmholtz instability mechanism (Boutilier & Yarusevych, 2012; Marxen *et al.*, 2013). The later stages of amplification lead to turbulent breakdown through the development of three-dimensional structures. Many studies focused on stability of LSBs involve either periodic (Jones *et al.*, 2010) or impulsive (Gaster & Grant, 1975; Michelis *et al.*, 2017) forcing. The majority of the available experimental investigations involved the two-dimensional description of the bubble topology in the streamwise plane. In comparison, the description of the spanwise evolution of coherent structures in LSBs has been considered only in a limited number of studies (e.g. Burgmann *et al.*, 2006).

This work focuses on the characterisation of a LSB under natural and forced conditions. Repetitive forcing of the LSB by means of a Dielectric Barrier Discharge (DBD) plasma actuator is applied in order to characterise the effect of natural and forced perturbations on the bubble dynamics. The emphasis is placed on the description of the spanwise flow development, where strong three dimensional effects are expected in the aft portion of the bubble (Marxen *et al.*, 2013). The disturbance is introduced locally and in a two-dimensional manner. The resulting spatial and temporal response of the flowfield is captured with streamwise and spanwise time-resolved Particle Image Velocimetry (PIV) measurements.

EXPERIMENTAL SETUP

Experiments are carried out in a closed-loop wind tunnel with square cross-section of 610mm$\times$610mm. A NACA0018 airfoil of 200mm chord is inserted in the test section (figure 1). The airfoil is set at a geometric and aerodynamic angle of attack of 4° while the pressure side boundary layer is tripped by means of a three-dimensional roughness strip. This is done in order to avoid unsteady effects as well as trailing edge tonal noise emission. A Cartesian coordinate system is defined with the origin at the leading edge of the airfoil. The x, y and z axes correspond to streamwise, wall-normal and spanwise direction respectively. The freestream velocity is set to $U_\infty = 9.2\mathrm{m/s}$ resulting in a Reynolds number based on the chord of $Re_c = 126,000$. At this speed, the freestream turbulence intensity

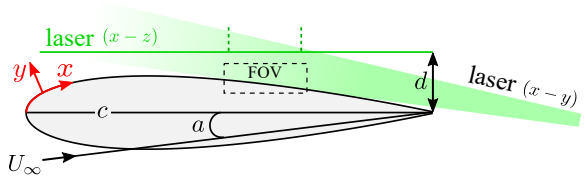

Figure 1. Experimental arrangement. The green dashed vertical lines denote the streamwise extent of the spanwise field of view (FOV).

is approximately 0.1%. For the selected conditions, a laminar separation bubble forms on the suction side, with mean separation and reattachment points are at $x/c \approx 0.35$ and 0.53, respectively.

The laminar boundary layer is perturbed two-dimensionally by means of an Alternating Current Dielectric Barrier Discharge (AC-DBD) plasma actuator (Corke *et al.*, 2010; Kotsonis, 2015). It consists of two asymmetrically placed self-adhesive copper electrodes separated by a *Kapton*® dielectric layer. The electrodes are 10mm wide in the streamwise direction, 30μm thick and 300mm long in the spanwise direction, while the dielectric barrier is 120μm thick. The discharge gap is located at $x/c = 0.3$, upstream of the separation point. The forcing signal is comprised of repetitive short pulses that are constructed by modulating a 3.5kV_{pp} and 5kHz sinusoidal carrier signal with a square signal of selected frequency. The modulation duty cycle is adjusted in regards to the pulse frequency, resulting in a pulse width of 1ms.

Time-resolved Particle Image Velocimetry (PIV) measurements are carried out by employing two *Photron SA4* high-speed cameras with 200mm Nikkor macro lenses, set at an aperture of $f/5.6$. Illumination is performed by a *Photonics DM20-527* Nd:YLF laser, whose beam is transformed to an approximately 2mm thick light sheet. A smoke generator uses water-glycol mixture to provide particle seeding.

Two fields of view are captured at an acquisition frequency of 2kHz. The first lies in the $x-y$ plane, at the airfoil midspan and is constructed by stitching images from both cameras, covering a field-of-view of 65mm × 22mm. The second view lies in the $x-z$ plane, parallel to and at a distance of $d = 21$mm from the airfoil chord, capturing a field-of-view of 56mm × 56mm (figure 1). In both cases, the acquired image pairs are processed with the *LaVision Davis 8.2* software using the multi-step interrogation algorithm (Scarano & Riethmuller, 2000) from an initial window of 48×48 pixels to a final of 16×16 pixels with 75% overlap. As a result, vector fields of 161×473 and 247×247 vectors are obtained for side and top views, respectively.

The results are presented on a surface-attached coordinate system (figure 1). The x coordinate runs tangent to the airfoil surface with an origin at the leading edge, while the y coordinate is normal to the local tangent and is measured from the airfoil surface (figure 1). The required scaling and geometric transformation of the vector fields (dewarping) is applied to all instantaneous realisations of the measurements in the $x-y$ plane. For the $x-z$ plane measurements, no dewarping is applied. The z coordinate is running parallel to the airfoil leading edge, with an origin at the midspan of the model.

RESULTS

Unforced bubble

All the results presented in this section pertain to $Re_c = 126,000$ and an angle of attack of $\alpha = 4°$. All dimensional variables are non-dimensionalised using the airfoil chord ($c = 0.2$m) and the freestream velocity ($U_\infty = 9.2$m/s).

Figure 2 presents time-average velocity and velocity fluctuation fields for the unforced LSB, serving as the baseline for the present study. The velocity field in the streamwise $(x-y)$ plane is shown in figure 2a along with the time-average dividing streamline, indicating the outline of the LSB. The general topology of the bubble follows the well known definition of short LSBs by Gaster (1967). It is evident that the mean separation point is not captured within the measurement domain. This is a necessary compromise for achieving sufficient spatial resolution in the reattachment region of the bubble. Nevertheless, an approximation of the mean separation point can be produced, capitalising on the nearly linear slope of the dividing streamline in the fore region of the bubble. Based on the extrapolated estimate of the mean separation point ($x_{\text{s}}^{\text{b}} = 0.29$) and the mean reattachment point ($x_{\text{r}}^{\text{b}} = 0.54$), the mean bubble length is estimated to be $l^{\text{b}} = 0.25$. The maximum bubble height is $h^{\text{b}} = 0.07$ and is located at $x = 0.48$.

Figures 2b and 2c demonstrate the standard deviation of streamwise (σ_u) and wall normal (σ_v) fluctuating velocity fields respectively. The appearance of strong streamwise and wall-normal fluctuations in the aft portion of the bubble is attributed to vortex shedding, in line with previous investigations on short LSBs (Yarusevych & Kotsonis, 2017). In particular, the topological arrangement of the streamwise fluctuations (figure 2b) reveals two distinct maxima in the vicinity of the maximum bubble height ($x \approx 0.5$). In conjunction with the single maximum in wall-normal fluctuations located approximately along the mean displacement thickness (figure 2c), the overall organisation of the unsteady fluctuating fields in the streamwise plane suggests the existence of coherent vortical shedding in the aft-portion of the bubble (Hain *et al.*, 2009).

Figure 2d presents the time-average velocity field in the spanwise $(x-z)$ plane. As mentioned earlier, the laser sheet in the $x-z$ plane was placed parallel to the chord of the airfoil. As such the distance of the spanwise measurement plane from the airfoil surface is not constant along the streamwise direction, due to the curvature of the airfoil. In the transformed and projected streamwise plane (dewarped $x-y$ plane) the measured $x-z$ plane assumes a curved shape. The intersection of the measured $x-z$ plane with the $x-y$ plane is indicated in figure 2 by a dash-dotted line.

The time-average flow on the $x-z$ plane demonstrates a high degree of two-dimensionality along the span (figure 2d). The streamwise component of velocity is uniformly decelerating along the x direction while the spanwise component is near-zero as evident by the quiver plot in figure 2d. The overall behaviour of the time-average velocity in the $x-z$ measurement plane confirms the establishment of spanwise invariant test conditions within the FOV. In contrast, the both streamwise (σ_u) and spanwise (σ_w) velocity fluctuations (figures 2e and 2f) reveal pronounced spanwise modulation. The combination of a highly two dimensional mean flow (figure 2d) and pronounced spanwise modulation of the fluctuating field topology in the aft portion of the bubble merits further analysis.

In order to quantify the spectral content of the dominant velocity fluctuations in the aft portion of the bubble,

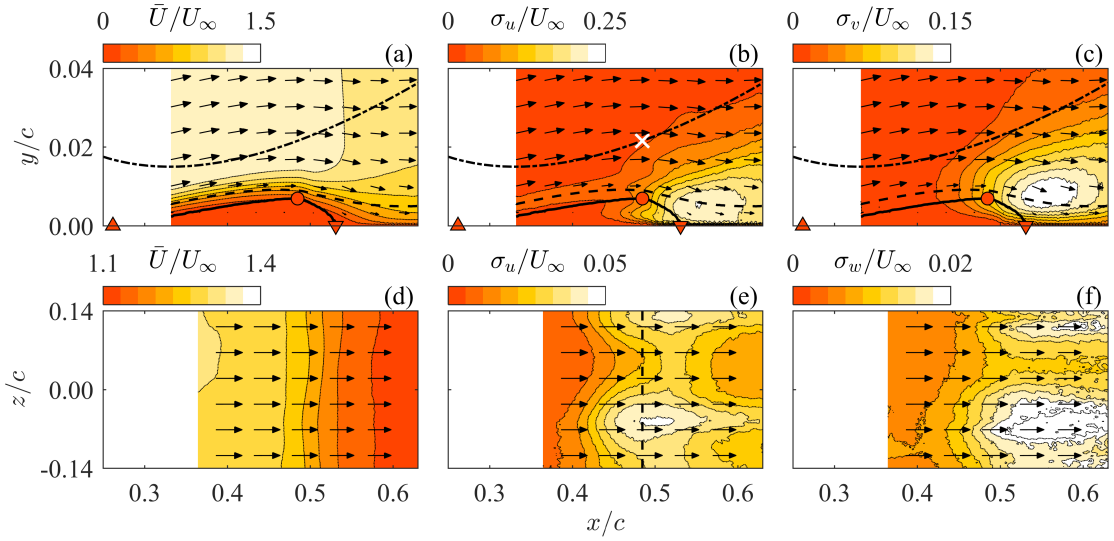

Figure 2. Time-averaged velocity field of the unforced bubble in the (a) $x-y$ plane and (d) $x-z$ plane. Standard deviation of the velocity fluctuations in the (b-c) $x-y$ plane and (e-f) $x-z$ plane. $\triangle$, $\bigcirc$ and $\triangledown$ denote mean separation, maximum height and reattachment respectively. Thick black line denotes dividing streamline and dashed line denotes displacement thickness. Black dash-dotted line denotes intersection of the $x-y$ and $x-z$ planes. White marker and vertical dashed line denote location of velocity probes for spectral analysis of figure 3.

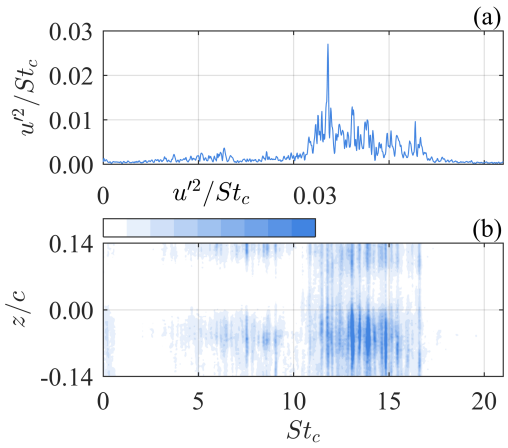

Figure 3. PSD of u' in the (a) $x-y$ plane and (b) $x-z$ plane for the unforced case. Probe locations are indicated in figure 2.

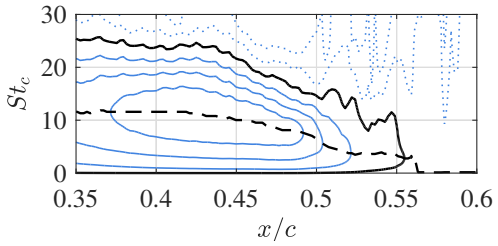

Figure 4. LST stability curve for the unforced case. Black line denotes neutral curve ($\alpha_i = 0$). Dashed line denotes locus of most unstable modes. Contour spacing is 0.1

the time-resolved PIV measurements are capitalised. Power Spectral Density (PSD) is computed using Welch's method from temporal signals of velocity components. Figure 3a demonstrates the PSD of the fluctuating streamwise velocity measured in the streamwise plane (PSD_{x-y}), with the probe location identified by a white marker in figure 2b. In order to facilitate a comparison between the streamwise and spanwise measurement planes, the streamwise location of the probe corresponds to the location of the maximum bubble height and the wall-normal location corresponds to the intersection of the two planes. The spectrum in figure 3a suggests that velocity fluctuations in the aft portion of the bubble are associated with a relatively narrow band of frequencies laying within $12 < St = fc/U_\infty < 17$. Additionally, a highly energetic discrete peak appears at $St \approx 11.8$ corresponding to a physical frequency of 542 Hz.

The presence of a confined frequency band of unsteady fluctuations in the aft-portion of the bubble suggests a selective amplification mechanism attested to the natural stability characteristics of the flow. This can be elucidated with the use of Linear Stability Theory (LST) analysis (Mack, 1984). The LST analysis is performed through solutions of the Orr-Sommerfeld equation, governing the development of small-amplitude perturbations in a time-invariant parallel flow. It has to be noted here that both assumptions of small perturbation amplitude and parallel flow are challenged by the inherent features of the bubble. Nevertheless, previous studies have demonstrated the applicability of LST as a diagnostic tool for accessing the stability of LSBs up to considerably late stages of transition (Michelis *et al.*, 2017).

In the present study, the experimentally measured time average PIV flowfield in the streamwise ($x-y$) measurement plane is used as the mean base flow for the LST analysis. The Orr-Sommerfeld eigenvalue problem is solved in spatial formulation where the real local Reynolds number (i.e. based on the x location) and frequency are used as known inputs. The eigenvalue is produced in the form of a complex wavenumber (α). The imaginary part of the wavenumber corresponds to the non-dimensional local growth rate (α_i) associated with a given frequency. Negative values of α_i denote unstable (i.e. amplifying)

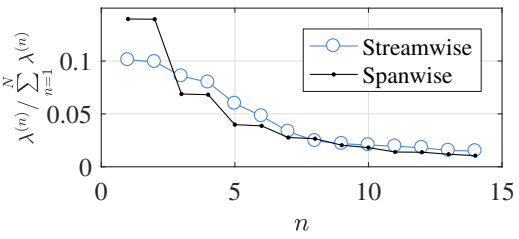

Figure 5. Relative POD eigenvalues of the unforced case.

modes while positive values of α_i denote stable (i.e. damping) modes. Neutral modes correspond to zero imaginary wavenumber.

The LST results for the baseline flow are shown in figure 4 in the form of a stability curve diagram. The flow is unstable at the upstream boundary of the measured FOV. The band of unstable frequencies spans from $St_c \approx 0$ to $St_c \approx 25$ in a streamwise range of $0.35 < x/c < 0.45$. The contour levels within the unstable region indicate the local growth rate (α_i) and the locus of the most unstable modes is denoted in figure 4 by the dashed black line. In the region upstream of the maximum bubble height ($0.35 < x/c < 0.45$) the most unstable frequency remains approximately constant at $St_c \approx 11$. This corresponds directly with the spectral peak in figure 3, linking the dominant velocity fluctuations in the aft portion of the bubble to the growth of natural instabilities along the incoming boundary layer and the separated shear layer (Marxen *et al.*, 2013).

The respective PSD of streamwise fluctuating velocity components measured in the spanwise ($x-z$) plane is shown in figure 3b. The corresponding velocity signals were probed along the span (dashed line i figure 2b) at the same streamwise location as that used for figure 3a. These are indicated with the vertical dashed line in figure 2d. The results indicate that the power of fluctuations along the z direction is modulated in accordance with the topological distribution of fluctuating velocity fields noted earlier in figures 2e and 2f. Nevertheless, despite the apparent modulation of the fluctuation power, the corresponding frequency band and centre frequency appear largely invariant along z, closely following the respective band in the $x-y$ plane (figure 3a) and the LST predictions (figure 4). The results in figure 3 suggest that while there is strong three-dimensionality in the spatial topology of the fluctuating velocity field in the breakdown region of the bubble (figures 2e-f), the dominant velocity fluctuations are associated with a common frequency band, evident in both streamwise and spanwise measurement planes. This implies that vortical structures shed in the aft portion of the bubble develop a consistent spanwise modulation.

Proper Orthogonal Decomposition (POD) is utilised to reveal the presence and topology of the dominant coherent structures in the LSB. For the present study, the snapshot method originally proposed by Sirovich (1987) is employed using the ensemble of instantaneous snapshots acquired by PIV. Figure 5 shows the relative energy (λ) of the fourteen most energetic spatial modes in both streamwise and spanwise measurement planes. For both planes, the energy cascade reveals two pairs of modes dominating the fluctuating velocity field. The cumulative energy of these first four modes is 37% of the total fluctuating energy for the streamwise plane and 42% for the spanwise plane. A careful inspection of the respective POD eigenfunctions reveals that the four most energetic modes for each measurement plane

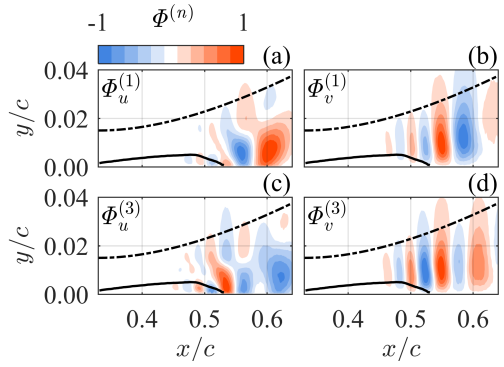

Figure 6. Normalised POD eigenfunctions in the $x-y$ plane for the unforced case. Same notation as figure 2.

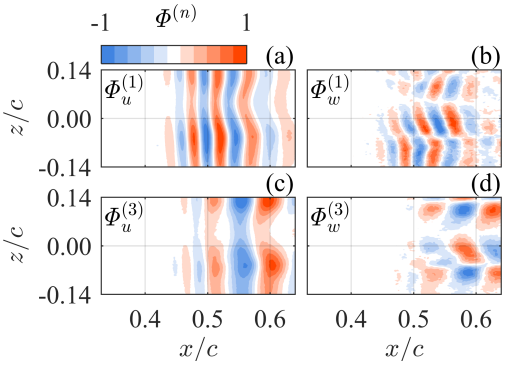

Figure 7. Normalised POD eigenfunctions in the $x-z$ plane for the unforced case.

represent pairs of harmonically coupled modes. The harmonic coupling manifests in the form of a $\pi/2$ phase shift between the POD modes of each pair, a necessary condition for convective structures. As such, the following analysis will focus on one spatial mode per harmonic mode pair, i.e the first and third most energetic POD mode per measurement plane. Figures 6 and 7 show the spatial modes in the streamwise and spanwise plane respectively. An important note to be made here is that the measurements and subsequent POD analysis between the two measurement planes are uncorrelated. As such, there is no direct correspondence between POD modes in the $x-y$ plane and POD modes in the $x-z$ plane other than their energy sorting. Subsequent analysis will treat the two planes independently. To be noted that all spatial POD modes are normalised to their respective maximum.

The structure of the spatial POD modes $\Phi^{(1)}$ and $\Phi^{(3)}$ shown in figure 6 corroborate the topology of the velocity fluctuations (figure 2b-c) and confirm the existence of coherent shedding in the aft portion of the bubble. This is further elucidated in figure 7 which shows the spatial arrangement of modes $\Phi^{(1)}$ and $\Phi^{(3)}$ in the spanwise plane. As previously conjectured, the POD modes confirm the existence of spanwise oriented vortical structures which undergo three-dimensional modulation in the streamwise direction. This is evident from distinct spanwise modulations in the streamwise component of the spatial modes (figures 7a and c) as well as the existence of a distinct spanwise organisation in the spanwise component (figures 7b and d). Additionally, it is striking to note the differences in the characteristic wavelengths between the first mode pair ($\Phi^{(1)}$) and the second mode pair ($\Phi^{(3)}$). This suggests the exis-

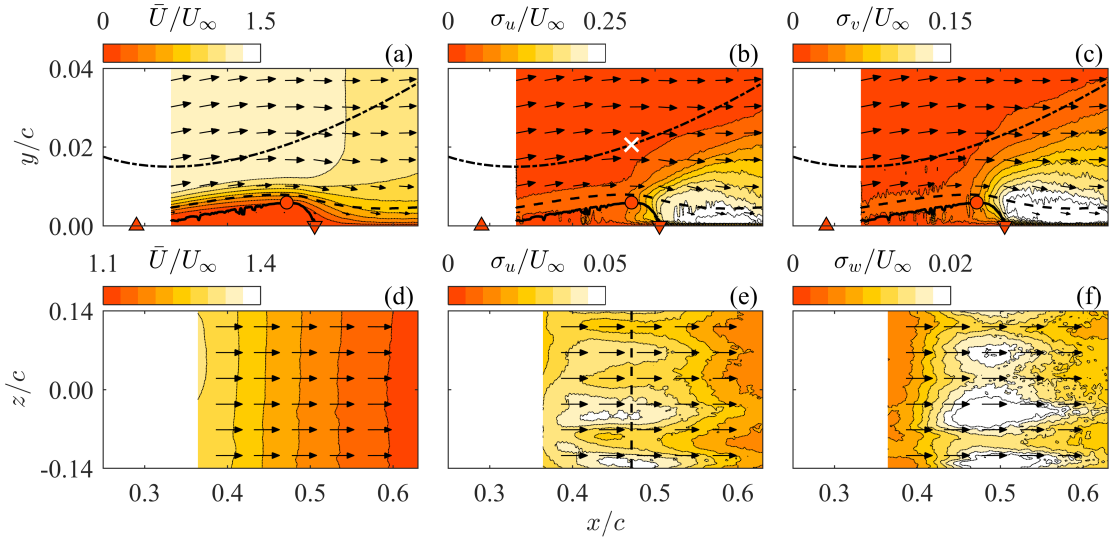

Figure 8. Statistic quantities of the forced LSB. Same notation as figure 2.

tence of multiple modes active in this region, supporting the previously discussed spectral measurements (figure 3).

Forced bubble

In order to investigate the origin of distinct spanwise deformations of dominant coherent structures, the bubble is conditioned using deterministic impulsive forcing by means of the installed plasma actuator. The frequency of successive pulses is chosen to be within the band of unstable modes predicted by the LST analysis (figure 4) at $St = 13$ ($f = 600$Hz). The time average velocity and velocity fluctuation fields for the forced bubble are shown in figure 8. In comparison to the baseline case (figure 2), forcing evidently results in the reduction of the bubble length to approximately 80% and the reduction of the maximum height to approximately 85% of the respective unforced values. This attributed to enhanced levels of velocity fluctuations in both streamwise (figure 8b-c) and spanwise (figure 8e-f) planes, indicating higher amplitude of perturbations and earlier transition. An inspection of the spanwise plane measurements reveals the sustainment of the strongly two dimensional mean flow. However, as for the baseline flow, the $x-z$ topology of σ_u reveals strong spanwise modulation for both streamwise and spanwise components (figures 8e and 8f).

The spectral analysis for the forced case has been applied in a similar fashion as for the unforced bubble. The PSD of the streamwise velocity fluctuations in the streamwise plane is shown in figure 9a. While the previously identified frequency band (figure 3a) is still visible, it is apparent that the majority of fluctuating power is now highly concentrated within a narrow band centred at $St_c = 13$, directly corresponding to the forcing frequency. This indicates the locking of the dominant velocity fluctuations on the actuation event. The spanwise spectral power distribution (figure 9b), further confirms the strong individuation concentration of the fluctuating energy along the span at the forcing frequency. Nevertheless, distinct spanwise modulation in the spectral content can be seen in figure 9b, similar to those observed for the baseline case (figure 3c).

The selection of a single coherent fluctuating mode in the spanwise plane due to the plasma forcing is further identified by the cascade of POD modal energy shown in figure 10. The first two POD modes in the spanwise plane are responsible for approximately 63% of the total fluctuating energy compared to 28% for the same modes in the unforced bubble. In contrast, the energy cascade in the streamwise plane appears to be weakly affected by the forcing.

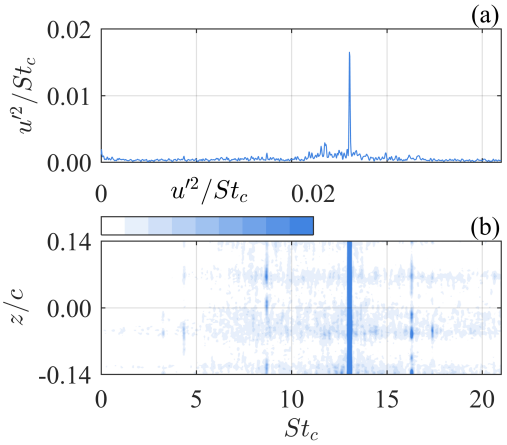

Figure 9. PSD of u' in the (a) $x-y$ plane and (b) $x-z$ plane for the forced case. Probe locations are indicated in figure 8

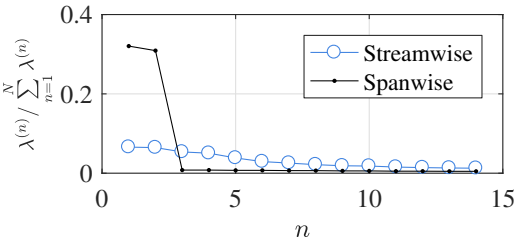

Figure 10. Relative POD eigenvalues for the forced case.

Further analysis of the spatial topology of the first and third POD modes for the streamwise and spanwise measurement planes is enabled by figures 11 and 12 respectively. As suggested by the energy cascade, minor differences can be

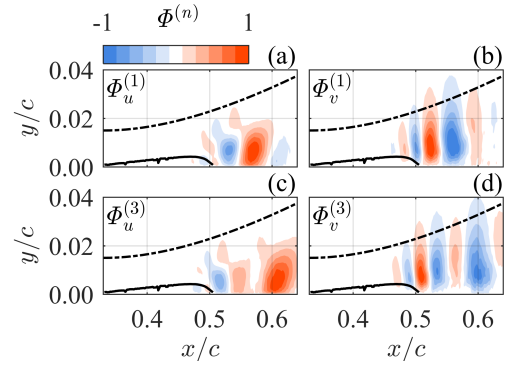

Figure 11. Normalised POD eigenfunctions in the $x-y$ plane for the forced case. Same notation as figure 2.

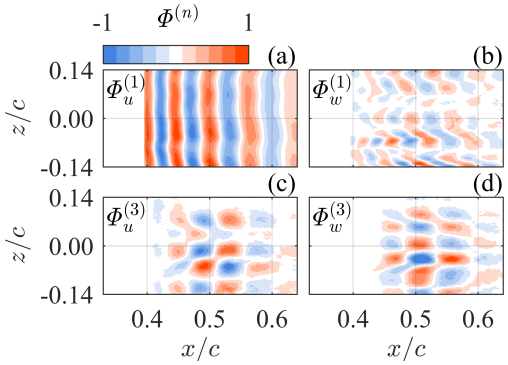

Figure 12. Normalised POD eigenfunctions in the $x-z$ plane for the forced case.

observed between the forced (figure 11) and unforced (figure 6) cases in the streamwise plane. In contrast, the topological effect of forcing on the POD modes in the spanwise plane is drastic. More specifically, in the $x-z$ plane, amplitude modulation is evident in both streamwise (figure 12a) and spanwise (figure 12b) vector components of the dominating mode, $\Phi^{(1)}$. Strong modulation is also apparent for $\Phi^{(3)}$, although it should be noted that the fluctuating energy content of this mode is only 0.8% of the total turbulent kinetic energy. The characteristic spanwise wavelength of the observed modulations decreased compared to that seen for the baseline case, likely due to the change in the streamwise wavenumber.

CONCLUSIONS

The present study investigated the spatial organisation of shedding structures in the aft-portion of a Laminar Separation Bubble. Statistical analysis reveals a rapid growth of velocity fluctuations, suggesting rigorous shedding and eventual transition. Spectral analysis confirms predictions of LST in identifying a band of unstable frequencies pertinent to the features of the baseline flow. POD analysis in the streamwise plane confirms the manifestation of vortex shedding in the aft portion of the bubble. The POD analysis in the spanwise plane shows that, while the dominant modes are coherent and monochromatic, they develop a three dimensional amplitude and shape modulation in the spanwise direction. This is present under natural unforced conditions within an otherwise strongly two-dimensional baseline flow.

The LSB was further conditioned by two dimensional forcing applied upstream of mean separation using a plasma actuator near the most amplified frequency. Under forcing, the shedding process locks to a single mode, while the coherency in the spanwise plane increases considerably. Nevertheless, distinct spanwise deformation of the dominant structures persists in the forced case. The aforementioned effect provides insight into the origin of three-dimensional breakdown in LSBs. More specifically, while related to the development of disturbances upstream of separation, spanwise deformation of dominant rollers developing in the separated shear layer is linked to the characteristics of these structures, persisting in both natural and forced bubbles.

REFERENCES

Boutilier, M. S. H. & Yarusevych, S. 2012 Separated shear layer transition over an airfoil at a low Reynolds number. *Physics of Fluids* **24** (084105).

Burgmann, S., Brücker, C. & Schröder, A. 2006 Scanning PIV measurements of a laminar separation bubble. *Experiments in Fluids* **41**, 319–326.

Corke, T. C., Enloe, C. L. & Wilkinson, S. P. 2010 Dielectric barrier discharge plasma actuators for flow control. *Annual Review of Fluid Mechanics* **42**, 505–529.

Gaster, M. 1967 The Structure and Behaviour of Laminar Separation Bubbles. *Tech. Rep.* 3595. Aeronautical Research Council Reports and Memoranda.

Gaster, M. & Grant, I. 1975 An experimental investigation of the formation and development of a wave packet in a laminar boundary layer. In *Proceedings of the Royal Society of London A: Mathematical, Physical and Engineering Sciences*, , vol. 347, pp. 253–269.

Hain, R., Kähler, C. J. & Radespiel, R. 2009 Dynamics of laminar separation bubbles at low-reynolds-number aerofoils. *Journal of Fluid Mechanics* **630**, 129–153.

Jones, L. E., Sandberg, R. D. & Sandham, N. D. 2010 Stability and receptivity characteristics of a laminar separation bubble on an aerofoil. *Journal of Fluid Mechanics* **648**, 257–296.

Kotsonis, M. 2015 Diagnostics for characterisation of plasma actuators. *Measurement Science and Technology* **26** (9).

Mack, L. M. 1984 Boundary-layer linear stability theory. *Tech. Rep.* 709. AGARD.

Marxen, O. & Henningson, D. S. 2011 The effect of small-amplitude convective disturbances on the size and bursting of a laminar separation bubble. *Journal of Fluid Mechanics* **671**, 1–33.

Marxen, O., Lang, M. & Rist, U. 2013 Vortex formation and vortex breakup in a laminar separation bubble. *Journal of Fluid Mechanics* **728**, 58–90.

Michelis, T., Kotsonis, M. & Yarusevych, S. 2017 Response of a laminar separation bubble to impulsive forcing. *Journal of Fluid Mechanics* **[In production]**.

Scarano, F. & Riethmuller, M.L. 2000 Advances in iterative multigrid PIV image processing. *Experiments in Fluids* **29** (SUPPL. 1), S51–S60.

Sirovich, L. 1987 Turbulence and the dynamics of coherent structures. I - Coherent structures. II - Symmetries and transformations. III - Dynamics and scaling. *Quarterly of Applied Mathematics* **45**, 561–571, 573–590.

Yarusevych, S. & Kotsonis, M. 2017 Effect of Local DBD Plasma Actuation on Transition in a Laminar Separation Bubble. *Flow, Turbulence and Combustion* pp. 1–22.